Fractional Topological Phases and Broken Time-Reversal Symmetry in Strained Graphene

Pouyan Ghaemi, Jérôme Cayssol, D. N. Sheng, Ashvin Vishwanath

Fractional Topological Phases and Broken Time-Reversal Symmetry in Strained Graphene

Pouyan Ghaemi,[1,2,3,*] Jérôme Cayssol,[2,4,5] D. N. Sheng,[6] and Ashvin Vishwanath[2,3]

[1]*Department of Physics, University of Illinois, Urbana, Illinois 61801, USA*
[2]*Department of Physics, University of California-Berkeley, Berkeley, California 94720, USA*
[3]*Materials Sciences Division, Lawrence Berkeley National Laboratory, Berkeley, California 94720, USA*
[4]*Max-Planck-Institut für Physik Komplexer Systeme, Nöthnitzer Strasse 38, 01187 Dresden, Germany*
[5]*Université Bordeaux and CNRS, LOMA, UMR 5798, F-33400 Talence, France*
[6]*Department of Physics and Astronomy, California State University, Northridge, California 91330, USA*

(Received 28 January 2012; published 26 June 2012)

We show that strained or deformed honeycomb lattices are promising platforms to realize fractional topological quantum states in the absence of any magnetic field. The strain-induced pseudomagnetic fields are oppositely oriented in the two valleys and can be as large as 60–300 T as reported in recent experiments. For strained graphene at neutrality, a spin- or a valley-polarized state is predicted depending on the value of the on-site Coulomb interaction. At fractional filling, the unscreened Coulomb interaction leads to a valley-polarized fractional quantum Hall liquid which spontaneously breaks time-reversal symmetry. Motivated by artificial graphene systems, we consider tuning the short-range part of interactions and demonstrate that exotic valley symmetric states, including a valley fractional topological insulator and a spin triplet superconductor, can be stabilized by such interaction engineering.

DOI: 10.1103/PhysRevLett.108.266801 PACS numbers: 73.43.−f, 72.80.Vp, 73.22.Pr

Fractional quantum Hall (FQH) phases are macroscopic-scale manifestations of quantum phenomena with unique features including the fractional charge and statistics (Abelian or non-Abelian) of elementary excitations. This topological order originates from the strong Coulomb interactions between electrons moving in a partially filled Landau level induced by a strong magnetic field. Recently, Chern insulator models with a nontrivial flat band [1–3] were also shown to exhibit topological order in the absence of any magnetic field [4–9]. Those so-called fractional Chern insulators (FCIs) explicitly break time-reversal symmetry $\mathcal{T}$ as did the original Haldane model [10]. In contrast, fractional topological insulators (FTIs) [11–14] can be naively thought of as two copies of time-reversed Laughlin FQH states, thereby obeying time-reversal symmetry $\mathcal{T}$. Despite a few proposals [15,16], the experimental implementation of FCIs and FTIs remains very challenging.

Motivated by recent experimental advances [17,18], we introduce another route toward fractional topological phases making use of the gauge fields that can be generated in a deformed honeycomb lattice [19–21]. The associated effective magnetic fields are opposite in the two different valleys and therefore do not break the time-reversal symmetry $\mathcal{T}$ [19]. Indeed, a scanning tunneling spectroscopy study [17] confirmed that straining graphene could yield flat pseudo-Landau levels (PLLs) [20,21] with effective fields as high as 300 T in each valley. Most recently, by designing a molecular honeycomb grid of carbon monoxide molecules on top of a copper surface, Gomes *et al.* [18] were able to observe the linear dispersion of Dirac fermions in graphene and furthermore to generate nearly uniform pseudomagnetic fields as high as 60 T by deforming this grid [18]. Finally, other realizations of artificial graphene systems, in patterned GaAs quantum wells [22] or with cold atoms trapped in hexagonal optical lattices [23,24], also provide experimental platforms to create strong valley-dependent effective magnetic fields.

In this Letter, we first consider real graphene under strong pseudomagnetic fields generated by a mechanical strain. We investigate the interaction-driven phases in the $n = 0$ PLL using mean field and numerical exact-diagonalization. The unscreened Coulomb interaction stabilizes a valley-polarized Laughlin liquid at filling $2/3$ of the $n = 0$ PLL. This state breaks spontaneously time-reversal symmetry and is characterized by a finite-charge Hall effect. At the neutrality point, we predict that strained graphene has either spin-polarized or valley-polarized state, depending on the strength of the on-site interactions, with current estimates [25] favoring the former state. Second, we have investigated what type of interactions could destabilize the valley-polarized $2/3$ state toward a valley-symmetric (time-reversal invariant) FTI. It turns out that the $2/3$ state is rather robust for realistic interactions. Nevertheless, attractive local corrections to the Coulomb interaction can stabilize this valley FTI, which is a FTI where the valley plays the role of spin. Finally, further increase of the attractive interactions leads to a spin triplet superconductor. Since the reported effective magnetic field strengths are around 300 T [17] or 60 T [18], the predicted phases might conceivably be realized with larger energy gaps than those in FQH states under a real magnetic field.

Model.—The noninteracting part of our model has been proposed by Guinea *et al.* in order to realize PPLs in strain

graphene under zero magnetic field [20]. The corresponding tight-binding Hamiltonian reads

$$H_0 = \sum_{\mathbf{r}_i} \sum_{a=1,2,3} [t + \delta t_a(\mathbf{r}_i)][a^\dagger(\mathbf{r}_i) b(\mathbf{r}_i + \boldsymbol{\delta}_a) + \text{H.c.}], \quad (1)$$

where $\delta t_a(\mathbf{r}_i)$ is the strain-induced variation of the nearest-neighbor hopping amplitude (with respect to the unperturbed value $t \simeq 2.7$ eV) between A site at $\mathbf{r}_i$ and B site at $\mathbf{r}_i + \boldsymbol{\delta}_a$ of the bipartite honeycomb lattice [19]. The smooth deformation field $\delta t_a(\mathbf{r}_i)$ is chosen in such a way to produce a nearly uniform magnetic field with a valley-dependent sign [20,26]. The valley-dependent vector potential $\mathbf{A}_\xi(\mathbf{r}) = \xi \sum_{a=1,2,3} \delta t_a(\mathbf{r}) e^{i\mathbf{K}\cdot\boldsymbol{\delta}_a}$ minimally couples to linearly dispersing low-energy excitations near the Dirac points located at momenta $\xi\mathbf{K}$ with $\mathbf{K} = (4\pi/3\sqrt{3}a_0)\mathbf{e_x}$ and $\xi = \pm 1$, a_0 being the carbon-carbon bond length [19]. The uniform pseudomagnetic field induces a pseudo-Landau level electronic structure $E_n = \xi\sqrt{2e\hbar v_F^2 B|n|}$, where n is the relative integer labeling the nearly flat levels (see Supplemental Material [27]). Beside the macroscopic orbital degeneracy, each of those PLLs has a fourfold degeneracy associated with the spin and valley isospin degrees of freedom. In contrast to the full SU(4) symmetry of graphene in an external real magnetic field [28,29], the internal symmetry of strained graphene is SU(2) for the spin and only Z_2 for the valley degrees of freedom.

In this Letter, we study interaction effects within the partially filled zero-energy flat band ($n = 0$ PLL) created by strain. We consider the following interaction Hamiltonian on the honeycomb lattice:

$$H_{\text{int}} = \sum_{\mathbf{r}_i \neq \mathbf{r}_j} V(\mathbf{r}_i - \mathbf{r}_j) n(\mathbf{r}_i) n(\mathbf{r}_j) + U_0 \sum_{r_i} n(\mathbf{r}_i) n(\mathbf{r}_i) + U_{\text{NNN}} \sum_{\langle r_i, r_j \rangle} n(\mathbf{r}_i) n(\mathbf{r}_j), \quad (2)$$

where $V(\mathbf{r}_i - \mathbf{r}_j) = e^2/4\pi\epsilon|\mathbf{r_i} - \mathbf{r_j}|$ denotes the bare Coulomb potential, $n(\mathbf{r}_i)$ the fermion number operator on site $\mathbf{r}_i$, and $\langle \mathbf{r}_i, \mathbf{r}_i \rangle$ represents summation over all pairs of next-nearest-neighboring (NNN) sites. The bare Coulomb interaction is the dominant interaction due to the poor screening in neutral graphene. Nevertheless, we also allow arbitrary modification of the short-distance part of the Coulomb interaction by adding local on-site and NNN interactions with respective strengths U_0 and U_{NNN}. The nearest-neighbor interaction is not effective in the presence of strong pseudomagnetic field because in the zero-energy PLL the noninteracting wave functions are localized on a single sublattice (see Supplemental Material [27]). Interesting proposals for altering short-ranged interactions using substrates with momentum-dependent dielectric susceptibility have been discussed [30]. Unfortunately, the actual values of U_0 and U_{NNN} are not known in strained graphene, although first-principles calculations yield total on-site coupling $U_0 = 9.3$ eV and a small deviation $U_{\text{NNN}} \simeq -0.04e^2/4\pi\epsilon a_0$ of the NNN coupling from its bare Coulomb value in freestanding (and unstrained) graphene in zero magnetic field [25].

Fractionalized phases and superconductivity at $2/3$ *filling of then* $= 0$ *PLL.*—Fractional Hall states in graphene under an external magnetic field were reported experimentally [31–33]. Although strain produces flat PLLs, it is not evident that interactions can generate incompressible phases at fractional filling in time-reversal invariant strained graphene. We focus here on the $2/3$ filling of the fourfold degenerate $n = 0$ PLL. This $2/3$ filling has been studied so far in graphene sheets [34,35] and in GaAs Hall bilayers [36] under real magnetic field. In the present case of strained graphene, this particular filling allows for interesting possibilities including valley ferromagnetism (which breaks spontaneously time-reversal symmetry), valley symmetric topological states, and also superconductivity.

Real graphene: time reversal breaking FQH state in a single valley.—We first consider real graphene with the unscreened Coulomb interaction, namely $U_0 = U_{\text{NNN}} = 0$ in Eq. (2). Then the ground state is found to be a valley polarized FQH state both for spinless (Fig. 1) and spinfull (Fig. 2) electrons. This valley-polarized state breaks spontaneously the time-reversal invariance of the strained graphene Hamiltonian, and spins are in a singlet state as in the $2/3$ FQH states [34–36] obtained under real magnetic field. We have further checked that the Chern number is $2/3$ and that the three lowest energy states form a degenerated ground-state manifold. Due to the large values of strain-induced pseudomagnetic fields, this state may be realized with elevated energy scales, allowing for the stabilization of fragile states. In order to test quantitatively the robustness of the $2/3$ valley-polarized FQH state, we now vary the parameter U_{NNN} in the Hamiltonian Eq. (2). It turns out that the $2/3$ valley-polarized state is rather stable both in the spinless (Fig. 1) and spinfull (Fig. 2) cases. Nevertheless when U_{NNN} is sufficiently negative, exotic valley symmetric phases can also be realized as detailed below. For clarity we describe separately the spinless and spinfull cases.

Spinless fermions and valley fractional topological insulator (FTI).—Let us consider spinless electrons and decompose the NNN coupling of Eq. (2) into an interaction between opposite-valley electrons ($U^{\text{op}}_{\text{NNN}}$) and an interaction between same-valley electrons (U^{s}_{NNN}). We first tune the intervalley correlations ($U^{\text{op}}_{\text{NNN}}$) while $U^{s}_{\text{NNN}} = 0$ (but note that electrons in the same valley still interact via the bare Coulomb potential).

In some intermediate parameter range ($-0.73 < U^{op}_{\text{NNN}} < -0.58$), an interesting quantum phase emerges with nine nearly degenerated states forming a ground-state manifold (GSM) [Fig. 1(a), lines with symbols] which is well-separated from the higher energy states [Fig. 1(a), lines without symbols]. This valley-symmetric and ninefold

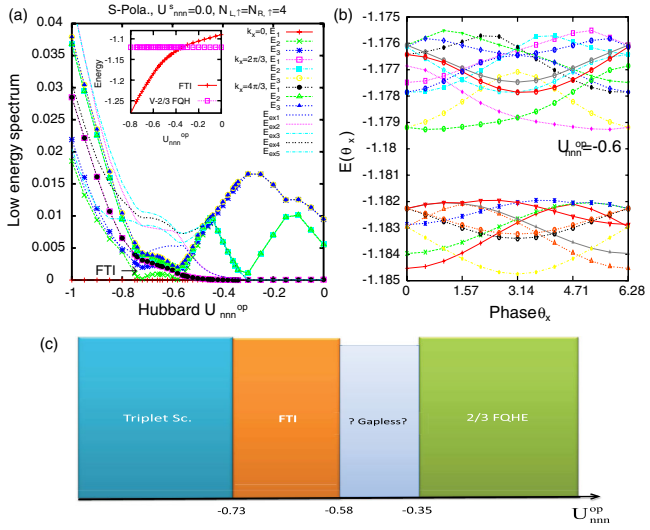

FIG. 1 (color online). The $n = 0$ PLL at fractional filling factor $\nu = -2 + 2/3$: spinless electrons. Upper panel left (a): low-energy spectrum as a function of the next-nearest-neighboring coupling $U^{\mathrm{op}}_{\mathrm{NNN}}$ between opposite valleys (deviation from the pure Coulomb value). In the region $-0.73 < U^{\mathrm{op}}_{\mathrm{NNN}} < -0.58$, the nine lowest energy states become close together and almost degenerated, thereby forming the ground-state manifold of the valley FTI. The inset shows the ground-state energies of the valley-polarized (V-2/3 FQH) and FTI states. Upper panel right (b): boundary-phase dependence and the robust gap between the GSM and higher-energy states for $U^{\mathrm{op}}_{\mathrm{NNN}} = -0.6$ inside the FTI phase. Lower panel (c): phase diagram as a function of $U^{\mathrm{op}}_{\mathrm{NNN}}$ for spinless electrons. Parameters for the exact diagonalization: The noninteracting orbitals are determined on a 24×24 lattice with a pseudomagnetic flux $\Phi_0/48$ per hexagon (see Supplemental Material [27]). The degeneracy of $n = 0$ PLL is $N_s = 12$ per spin direction and per valley. The low-energy spectrum is calculated for $N_e = 8$ ($N_L = N_R = 4$) electrons with polarized spin occupying those $N_s = 12$ states. Energies are given in units of $e^2/4\pi\epsilon a_0 \simeq 10$ eV.

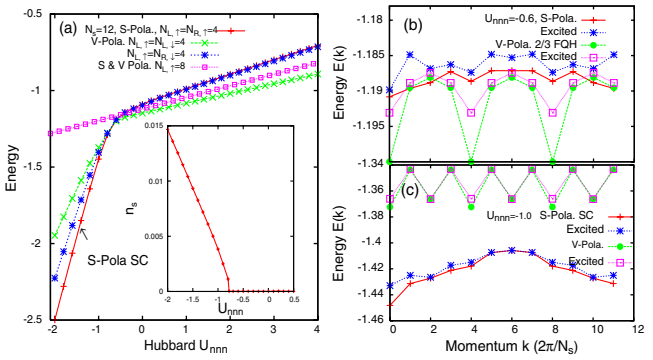

FIG. 2 (color online). The $n = 0$ PLL at fractional filling factor $\nu = -2 + 2/3$: spinfull electrons. Left panel (a): the energy of different ground states as a function of the next-nearest-neighboring coupling U_{NNN} defined in Eq. (2). In the range $U_{\mathrm{NNN}} > -0.8$, which includes the pure Coulomb interaction of realistic graphene ($U_{\mathrm{NNN}} = 0$), the ground state is a valley-polarized and spin singlet FQH state (green $\times$ crosses). Only a very significant attraction $U_{\mathrm{NNN}} < -0.8$ can destabilize this state toward a valley-unpolarized and spin-polarized superconducting state (red $+$ crosses). This superconducting phase is characterized by a finite superfluid density as shown in the inset. Right panel (b) and (c): two lowest energies in each momentum sector as a function of k for the valley-polarized state ($U_{\mathrm{NNN}} = -0.6$, upper) and for the spin-polarized superconductor ($U_{\mathrm{NNN}} = -1$, lower). Parameters for the exact diagonalization: same as in Fig. 1 but with the spin degree of freedom.

degenerated phase is called valley fractional topological insulator here, since valley plays the role taken by spin in the previously discussed "spin" FTIs [11–14]. Moreover the momentum quantum numbers of these states are at $k = 0$ and other k determined by shifting the momentum of each electron by an integer multiple of $2\pi/N_s$, where N_s is the PLL orbital degeneracy. This determines three different momenta sectors ($k = 0$, $\pi/3$, and $2\pi/3$) and there are three near degenerate states in each sector. These sectors can be considered as ground-state flows from one sector to another upon inserting flux through adding the twist boundary phase [Fig. 1(b)].

As a complementary characterization of the valley FTI phase, we further perform valley-pseudospin Chern number calculation [37,38] by adding the same boundary phase along the x-direction, and the opposite ones along the y-direction for both valleys [39,40]. This generalized pseudospin Chern number is well-defined as the electron number in each valley is conserved: thus the valley-pseudospin number is a is a good quantum number. We find a total Chern number quantized to 6 for all nine levels, characterizing the $2/3$ fractionalized valley spin-Hall effect.

Finally we can also turn on and increase the intravalley part of the NNN coupling U^s_{NNN} (see Supplemental Material [27]). In the limit of very large intravalley correlations ($U^s_{\mathrm{NNN}} \to \infty$), we expect a totally valley-decoupled $1/3 + 1/3$ phase consisting of two $1/3$ Laughlin FQH states with opposite chiralities. We find no phase transition between the valley FTI state discussed above (at $U^s_{\mathrm{NNN}} = 0$) and the decoupled fractional valley Hall insulator (see Supplemental Material [27]).

The above results for spinless electrons can be summarized in a phase diagram [Fig. 1(c)]. For $U^{\mathrm{op}}_{\mathrm{NNN}} > -0.35$ (which includes realistic graphene), electrons have a natural tendency toward valley ferromagnetism, which is expected for repulsive interactions in a such a flat band system. In order to realize the valley FTI, one needs to counteract this trend by tuning an attraction between electrons in the opposite valleys. Besides, one also notices a narrow range of parameters ($-0.58 < U^{\mathrm{op}}_{\mathrm{NNN}} < -0.35$) where the valley-polarization is lost but the GSM degeneracy not yet achieved. The understanding of this crossover region between the valley polarized FQH insulator and the valley FTI is still lacking and will be studied elsewhere. Finally superconductivity might appear when attraction is dominant ($U^{op}_{\mathrm{NNN}} < -0.58$). This flat band superconductivity is discussed below in more details for the spinfull electrons.

Spinfull fermions and spin triplet superconducting state.—We now consider spinfull fermions and we tune U_{NNN} without distinguishing the valleys. For sufficiently large attraction (Fig. 2), namely $U_{\mathrm{NNN}} \leq -0.8$ (note that when added to the Coulomb repulsion, this ends up giving a somewhat smaller but still attractive next-nearest neighbor interaction of $U_{\mathrm{NNN}}^{\mathrm{tot}} = -0.2$), the ground state of the spinfull model becomes a spin triplet and valley singlet superconducting state which is consistent with BCS-type mean field treatment (see Supplemental Material [27]). The superconductivity is characterized by a finite superfluid density $n_s = 1/2 \frac{\partial^2 E_g}{\partial \theta^2}$ which is calculated from the change of the ground-state energy E_g upon adding a small phase twist θ as [39–41]. Moreover the finite jump for n_s at the transition point $U_{\mathrm{NNN}} = -0.8$ (inset of Fig. 2) points toward a first-order transition between the valley-polarized state and the spin-polarized superconducting state. The typical momentum dependence of energy [Fig. 2(c)] differs drastically from the 2/3 valley-polatized FQH case [Fig. 2(c)] as the ground state is in the $k = 0$ sector without the typical quasidegeneracy of FQH state.

Half-filling $n = 0$ PLL.—We now turn to the case of neutral graphene (filling factor $\nu = 0$) under large pseudomagnetic fields generated by strain. Due to the electron-hole symmetry, the $n = 0$ PLL is half-filled and there is natural a competition between valley ferromagnet $\Psi_V = \prod_k c^\dagger_{R,k,\uparrow} c^\dagger_{R,k,\downarrow} |0\rangle$ and spin ferromagnet $\Psi_S = \prod_k c^\dagger_{R,k,\uparrow} c^\dagger_{L,k,\uparrow} |0\rangle$ ground states, k labeling the Landau orbitals of the zero-energy ($n = 0$) PLL and (R, L) the valleys. A Similar issue of valley and spin ferromagnetism in the half-filled $n = 0$ Landau level has attracted a lot of interest for unstrained graphene under a real magnetic field [28,29,42–45]. Here we revisit this problem in the case of a time-reversal symmetric pseudomagnetic field.

We first consider the case of pure Coulomb interaction ($U_0 = U_{\mathrm{NNN}} = 0$). Using Hartree-Fock method [28,29] we find that the valley- and spin-polarized states have the same energy only when dominant density-density terms are taken into account. We find that the intervalley backscattering terms lift this degeneracy by favoring the valley polarization. Note that for real magnetic field, those backscattering terms are absent in the zero-energy Landau level ($n = 0$) due to the symmetry of the eigenspinors [28,29]. Also contrary to the real magnetic field Hall effect, long-range Coulomb interaction prefers an Ising-like Z_2 valley-polarized state rather than a more general SU(2)-valley-rotated state (see Supplemental Material [27]).

We now introduce on-site Hubbard interaction U_0 where $U_{\mathrm{NNN}} = 0$ in Eq. (2) and compute numerically the total energy of finite-size systems on a torus (Fig. 3, squares). As expected solely the energy of the valley-polarized state is modified while the spin-polarized state is unchanged (Fig. 3, horizontal dashed line) because double occupancy is forbidden by the Pauli principle in the fully spin-polarized state. As a result, the competing valley-polarized state (Fig. 3, empty squares) is the ground state as long as

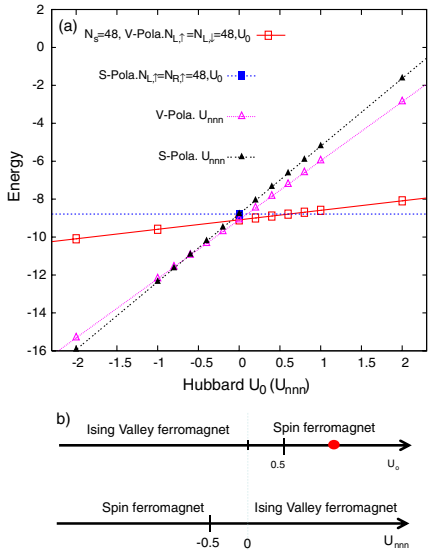

FIG. 3 (color online). Neutral graphene, $\nu = 0$. Upper panel (a): Hartree-Fock energies of the Ising valley-polarized (Ψ_V) and spin-polarized (Ψ_S) states as a function of the on-site Hubbard coupling U_0 whereas $U_{\mathrm{NNN}} = 0$ (squares). We have also plotted the Hartree-Fock energies as a function of U_{NNN} in the absence of on-site correlation, $U_0 = 0$ (triangles). Lower panel (b): corresponding phase diagrams. The energy is in units of $e^2/4\pi\epsilon a_0$, where a_0 is the distance between the nearest-neighbor sites. The red dot indicates the value of the coupling U_0 for freestanding and unstrained graphene according to Ref. [25]. Numerical parameters: The lattice we considered has 96×96 sites. The degeneracy of the PLL orbits was $N_s = 48$, and the electron number is $N_e = 96$.

the Hubbard interaction is not too repulsive ($U_0 < 0.5$ in units of $e^2/4\pi\epsilon a_0$), including the pure Coulomb case. Further increase of the on-site Hubbard interaction stabilizes the spin ferromagnet state. Using gating or different substrates, it could be possible to switch the ground state between spin ferromagnet and valley Ising ferromagnet. Spin-polarized STM and Kerr imaging could indeed detect these competing ground states. Here the valley Ising ferromagnet is an integer quantum Hall state with two units of quantized Hall conductance, that spontaneously breaks time-reversal symmetry.

In order to test the sensitivity of the phase diagram with respect to the details of the short-range part of the interaction, we further consider a second model where the next-nearest-neighboring coupling U_{NNN} is varied while $U_0 = 0$. Interestingly we have obtained the reverse phenomenology where repulsive U_{NNN} tends to valley polarize the system (Fig. 3, triangles).

Conclusion.—We have shown that strained graphene hosts various fractional topological phases which depend on the detailed structure of the electron-electron interactions. In current experiments on both real graphene [17] and artificially designed molecular graphene [18], the nanoscale strained regions are small, typically of the order of the magnetic length, and they are strongly coupled to a metallic substrate. Future experiments on insulating

substrates could address bigger strained regions. Nevertheless, signatures of fractional states in restricted domains and interactions with itinerant electrons outside the strained region will be important topics for future study. The $n = 0$ Landau levels are expected to be the best isolated, since they occur at the Dirac point, where the density of itinerant states is the smallest.

The predicted phases relies on the flatness of the PLL $n = 0$ which requires spatially homogeneous strained-induced magnetic fields in each valley. In this respect artificially patterned honeycomb lattices [18,22,46] potentially allows for a better control upon the deformation pattern and therefore upon the flatness of the PLLs, in comparison to the mechanical strain in real graphene. Cold atoms in hexagonal optical lattices [23,24] are particularly suitable to access the attractive interaction regime. Finally we stress that the long-range part of the Coulomb interaction is always present in our calculations. This is at odds with current experiments [17,18,23,24] but it should be relevant for real graphene and for future experiments on artificial graphenes realized in surface states lying on insulating substrates. Finally this study opens the prospect of discovering a series of new nontrivial topological phases at other fractional fillings and in higher pseudo-Landau levels as well.

We are grateful to J. Alicea and N. Regnault for useful comments. J. C. acknowledges support from EU/FP7 under Contract TEMSSOC and from ANR through Project No. 2010-BLANC-041902 (ISOTOP). This work is also supported by DOE Office of Basic Energy Sciences under Grant No. DE-FG02-06ER46305 (D. N. S.) and DE-AC02-05CH1123 (A. V.), the NSF Grant No. DMR-0958596 for instrument (D. N. S.), as well as the Laboratory Directed Research and Development Program of Lawrence Berkeley National Laboratory under US Department of Energy Contract No. DE-AC02-05CH11231 (P. G.). A. V. acknowledges hospitality from ICTS Bangalore where part of this work was completed. P. G. also acknowledges support from the institute for condensed matter theory at the University of Illinois at Urbana-Champaign.

Note added.—Recently, a study of nonzero PLLs in strained graphene [47], and related work on spin fractional topological insulators [48] appeared.

*pouyan@berkeley.edu

[1] E. Tang, J.-W. Mei, and X.-G. Wen, Phys. Rev. Lett. **106**, 236802 (2011).
[2] K. Sun, Z. Gu, H. Katsura, and S. Das Sarma, Phys. Rev. Lett. **106**, 236803 (2011).
[3] J. W. F. Venderbos, M. Daghofer, and J. van den Brink, Phys. Rev. Lett. **107**, 116401 (2011).
[4] T. Neupert, L. Santos, C. Chamon, and C. Mudry, Phys. Rev. Lett. **106**, 236804 (2011).
[5] D. N. Sheng, Z.-C. Gu, K. Sun, and L. Sheng, Nat. Commun. **2**, 389 (2011).
[6] Y.-F. Wang, Z.-C. Gu, C.-D. Gong, and D. N. Sheng, Phys. Rev. Lett. **107**, 146803 (2011).
[7] J-W. Mei, E. Tang, and X-G. Wen, arXiv:1102.2406.
[8] N. Regnault and B. A. Bernevig, Phys. Rev. X **1**, 021014 (2011).
[9] X.-L. Qi, Phys. Rev. Lett. **107**, 126803 (2011).
[10] F. D. M. Haldane, Phys. Rev. Lett. **61**, 2015 (1988).
[11] M. Levin and A. Stern, Phys. Rev. Lett. **103**, 196803 (2009).
[12] J. Maciejko, X.-L. Qi, A. Karch, and S.-C. Zhang, Phys. Rev. Lett. **105**, 246809 (2010).
[13] B. Swingle, M. Barkeshli, J. McGreevy, and T. Senthil, Phys. Rev. B **83**, 195139 (2011).
[14] T. Neupert, L. Santos, S. Ryu, C. Chamon, and C. Mudry, Phys. Rev. B **84**, 165107 (2011).
[15] D. Xiao, W. Zhu, Y. Ran, N. Nagaosa, and S. Okamoto, Nat. Commun. **2**, 596 (2011).
[16] J. Venderbos, S. Kourtis, J. van den Brink, and M. Daghofer, Phys. Rev. Lett. **108**, 126405 (2012).
[17] L. Levy, S. A. Burke, K. L. Meaker, M. Panlasigui, A. Zettl, F. Guinea, A. H. Castro Neto, and M. F. Crommie, Science **329**, 544 (2010).
[18] K. K. Gomes, W. Mar, W. Ko, W. Guinea, and H. C. Manoharan, Nature (London) **483**, 306 (2012).
[19] A. H. C. Neto, F. Guinea, N. M. R. Peres, K. S. Novoselov, and A. K. Geim, Rev. Mod. Phys. **81**, 109 (2009).
[20] F. Guinea, M. I. Katsnelson, and A. K. Geim, Nature Phys. **6**, 30 (2009).
[21] T. Low and F. Guinea, Nano Lett. **10**, 3551 (2010).
[22] A. Singha *et al.*, Science **332**, 1176 (2011).
[23] P. Soltan-Panahi, J. Struck, P. Hauke, A. Bick, W. Plenkers, G. Meineke, C. Becker, P. Windpassinger, M. Lewenstein, and K. Sengstock, Nature Phys. **7**, 434 (2011).
[24] L. Tarruell, D. Greif, T. Uehlinger, G. Jotzu, and T. Esslinger, Nature (London) **483**, 302 (2012).
[25] T. O. Wehling, E. Sasioglu, C. Friedrich, A. I. Lichtenstein, M. I. Katsnelson, and S. Blugel, Phys. Rev. Lett. **106**, 236805 (2011).
[26] A. Vaezi, N. Abedpour, and R. Asgari, arXiv:1105.5232.
[27] See Supplemental Material at http://link.aps.org/supplemental/10.1103/PhysRevLett.108.266801 for the noninteracting model and additional details on the interacting driven states.
[28] J. Alicea and M. P. A. Fisher, Phys. Rev. B **74**, 075422 (2006).
[29] M. O. Goerbig, R. Moessner, and B. Doucot, Phys. Rev. B **74**, 161407 (2006).
[30] Z. Papic, R. Thomale, and D. A. Abanin, Phys. Rev. Lett. **107**, 176602 (2011).
[31] K. I. Bolotin, F. Ghahari, M. D. Shulman, H. L. Stormer, and P. Kim, Nature **462**, 196 (2009).
[32] X. Du, I. Skachko, F. Duerr, A. Luican, and E. Y. Andrei, Nature **462**, 192 (2009).
[33] C. R. Dean, A. F. Young, P. Cadden-Zimansky, L. Wang, H. Ren, K. Watanabe, T. Taniguchi, P. Kim, J. Hone, and K. L. Shepard, Nature Phys. **7**, 693 (2011).
[34] C. Toke and J. K. Jain, Phys. Rev. B **75**, 245440 (2007).
[35] M. O. Goerbig and N. Regnault, Phys. Rev. B **75**, 241405 (2007).
[36] I. A. McDonald and F. D. M. Haldane, Phys. Rev. B **53**, 15845 (1996).

[37] D. J. Thouless, M. Kohmoto, M. P. Nightingale, and M. den Nijs, Phys. Rev. Lett. **49**, 405 (1982).
[38] Q. Niu, D. J. Thouless, and Y.-S. Wu, Phys. Rev. B **31**, 3372 (1985).
[39] D. N. Sheng, L. Balents, and Z. Wang, Phys. Rev. Lett. **91**, 116802 (2003).
[40] D. N. Sheng, Z. Y. Weng, L. Sheng, and F. D. M. Haldane, Phys. Rev. Lett. **97**, 036808 (2006).
[41] R. G. Melko, A. Paramekanti, A. A. Burkov, A. Vishwanath, D. N. Sheng, and L. Balents, Phys. Rev. Lett. **95**, 127207 (2005).
[42] L. Sheng, D. N. Sheng, F. D. M. Haldane, and L. Balents, Phys. Rev. Lett. **99**, 196802 (2007).
[43] I. F. Herbut, Phys. Rev. Lett. **97**, 146401 (2006).
[44] M. Goerbig, Rev. Mod. Phys. **83**, 1193 (2011).
[45] Y. Barlas, K. Yang, and A. H. MacDonald, Nanotechnology **23**, 052001 (2012).
[46] C. H. Park and S. Louie, Nano Lett. **9**, 1793 (2009).
[47] D. Abanin and D. A. Pesin, arXiv:1112.6420.
[48] H. Chen and K. Yang, Phys. Rev. B **85**, 195113 (2012).